Journal of Engineering Science and Technology
Vol. 18, No. 1 (2023) 671 - 684

PARAMETRIC STUDY OF SINGLE AIR BUBBLE RISING THROUGH DIFFERENT SALINITY WATER COLUMN USING VOLUME OF FLUID (VOF) TECHNIQUE

FARHAN L. RASHID [1], EMADQ.HUSSEIN [2],
AHMED KADHIM HUSSEIN[3], OBAI YOUNIS [4,5,*]

[1]Petroleum Engineering Department, College of Engineering,
University of Kerbala, Kerbala, Iraq
[2]Mechanical Engineering Department, College of Engineering,
University of Kerbala, Kerbala, Iraq
[3]Mechanical Engineering Department, College of Engineering,
University of Babylon, Babylon City, Iraq
[4]Department of Mechanical Engineering, College of Engineering in
Wadi Addwasir, Prince Sattam Bin Abdulaziz University, Al-kharj 11942 , KSA.
[5]Department of Mechanical Engineering, Faculty of Engineering, University of Khartoum, Sudan
*Corresponding author email: oubeytaha@hotmail.com

Abstract

The rising air bubbles in a liquid due to gravity has been researched for many years and remain a fascinating subject today. The 2-D Volume of Fluid (VOF) method and the CFD technique were employed for simulating. The dynamic meshing technique is applied to simulate the hydrodynamics of rising air bubbles in a liquid water column via the User Defined Function (UDF) code in the C++ environment was developed to evaluate bubble rising through the water column with different salinity. The rising of air bubble through a stagnant water column has been considered, and the influence of column dimension, bubble size, and aspect ratio on the rising velocity and some parameters (Reynolds number, Re, Eötvös number, Eo, Weber number, We, Morton number, Mo, Drag coefficient, C_D, Capillary number, Ca, and Flow number, F_N are investigated. The obtained results showed that the bubble rising velocity increases with the bubble size. The bubble shapes vary with the diameter due to the effect of varying drag forces.The drag coefficient is reduced from 2.85 to 0.4 as the Reynolds number increases from 20 to 1475.The maximum rising velocity increases by 75% when the Eötvös number increases from 700 to 950, while the Weber number increases by 60% when the bubble size increases from 5 to 7 mm. A good agreement was obtained between the rising velocity predicted in the simulation and that obtained from the literature.

Keywords: Air bubble, Dynamic mesh, Rising Velocity, Salinity Water, VOF.

1. Introduction

Water is used to cool most industrial operations, including refineries, petrochemical plants, Liquefied Natural Gas LNG plants, and power plants. Big amounts of saltwater are utilized as cooling media in large industrial plants, and the capacity becomes several ten thousand cubic meters per hour. In a seawater cooling system of large industrial plants, the seawater, after passing the heat exchanger, is usually discharged to the sea zone during a discharge pipe and a discharge basin [1].

In real-world industrial operations, a large number of bubbles of various forms, sizes, and speeds interact with one another in the instrument. The engineering implementation (salinity water desalination, nuclear reactor cooling, heat exchanger, and solar collector) is mostly based on the features of bubbles and the interaction between the scattered and continuous phases [2, 3]. Furthermore, due to the intricacy of their motion characteristics, the motion of many bubbles differs from that of single bubbles. Consequently, studying the characteristics of bubble movement and their interactions is useful and academically relevant in a range of engineering fields [4-12].

High-speed photographic and probe technology are now the most used testing procedures. Because probe technology [13] requires direct contact with the gas phase to measure gas hold-up and bubble size in the system, high-speed photography has become increasingly important for measuring bubble behavior characteristics due to its advantages of full-field, non-contact, and instantaneous measurement [14]. Islam et al. [15] utilized the CFD code FLUENT to numerically analyse the rising of single gas bubble behavior through sluggish (stagnant) water in a trapezoidal and rectangular domain. Pradeep et al. [16] proposed 3-D bubble dynamics on the Open FOAM platform. The verified numerical model was utilized to analysed hydrodynamics of a single bubble in sodium to show a similarity between the two systems. In the sodium system, the aspect ratio of the bubble of 0.9 cm diameter is found to be quite similar to that of a 0.5 cm bubble in the water system. Nguyen et al. [17] looked into how contaminants affected the rise of liquid droplets in other liquids. The characteristics of rising multiple CO_2 droplets contaminated with SO_2 in a situation where they could leak into seawater from the facility or a pipeline in a Carbon Capture and Storage (CCS) venture are examined.

Bubble properties of bubbly foam of subcooled flow boiling in made-up seawater are measured by Li et al. [18], involving bubbles Sauter mean diameter, bubble form, bubbles equivalent diameters, bubble size distribution, and bubbles directions. According to the findings, the mean diameter of Sauter of purified water might be 16-30% bigger than that of made-up saltwater.

Suyantara et al. [19] investigation aimed to see how saltwater affected bubble-particle interaction with molybdenite and chalcopyrite surfaces. In artificial seawater, it was discovered that kerosene absorbed at the bubble's air/liquid interface lowered the bubble rise velocity and increased the bubble aspect ratio. Ramirez et al. [20] investigated the effects of bubbles-oily and the sodium silicate (SS) and dispersants sodium hexametaphosphate (SHMP) on molybdenite flotation in alkaline seawater. The obtained results reveal that when kerosene is applied to the bubble's surface, molybdenite recovery rises, especially in the molybdenite flotation at pH > 9.5 in saltwater.

The influence of release size, current velocity, and release rate on CO_2 gas-seawater dispersion was studied by Pham et al. [21]. The study found that a high release rate during low current had the most serious consequences. Straatman and van Sark [22] presented a low-cost technique for indirectly capturing and purifying CO_2 from ocean water. According to Henry's law, atmospheric CO_2 dissolves in saltwater. The calculation shows non-condensable cold water containing up to 14% CO_2.

According to the literature survey, the hydrodynamics of a single air bubble through stagnant water with different salinity was not reported in the literature. As a result, this research aims to implement the theoretical investigation of different air bubble sizes raised in stagnant water with different salinity using the Volume of Fluid (VOF) method and the CFD technique. The research findings might aid in understanding the design of a water column and real physical phenomena. Finally, it proposes innovative criteria for selecting the multiphase flow model on CFD simulation.

2. Mathematical Model

2.1. Case study

In this work, the 2-D domain is employed to explore the rising single air bubble behavior in the stagnant water column with different salinity. The dimensions of the column are width of (20-40) mm and height of (100-150) mm, as presented in Fig. 1. The single air bubble is decreed at the center and a height of 10 mm from the base of the column at the first stage of simulation. Four bubble diameters of 5, 6, and 7 mm are studied in this work. The compliant water's air bubble will raise under the buoyancy force action [23].

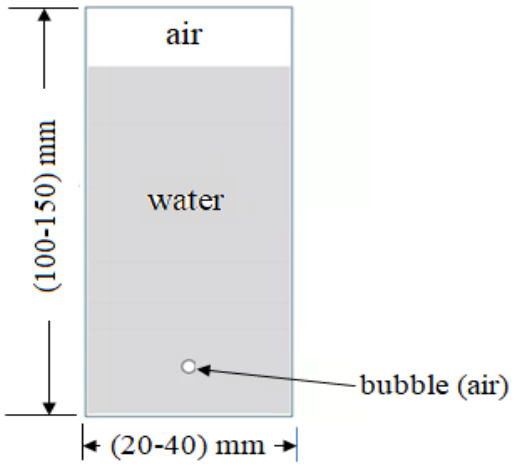

Fig. 1. Schematic of possible flow regimes in bubble columns.

In this work, the primary phase is water (liquid), be natural at once and with different salinity in others, and the secondary phase is air (gas). The main physical properties used to observe and describe the matter of the single air and water are tabulated in Table 1 [24].

Table 1. Atmospheric conditions physical characteristics of test fluids [24].

Fluid	Air	Water
Density, kg/m^3	1.22	999
Viscosity, Pa.s	0.018	0.89
Surface tension, mN/m	-	72.0

2.2. Governing equations and modeling

A comprehensive CFD model has been utilized in this article to cover all features of two-phase flow during the operation of a rising single air bubble through stagnant water with different salinity. A user-defined function has been used to finish the Fluent code to mimic the phase change material.

The Reynolds number (Re), Eötvös number (E_o), Weber number (W_e), Morton number (M_o), Drag coefficient (C_D), Capillary number (C_a), and Flow number (F_N) are the parameters that characterize the Air Bubble Rising Through Different Salinity Water Column, as revealed by the steady-state momentum and energy equations [23-25].

$$\mathrm{Re} = \frac{\text{inertial force}}{\text{viscous force}} = \frac{\rho_l u_b d}{\mu_l} \quad (1)$$

$$\mathrm{E_o} = \frac{\text{buoyancy force}}{\text{surface tension force}} = \frac{\rho_l g d^2}{\sigma} \quad (2)$$

$$\mathrm{W_e} = \frac{\text{inertial force}}{\text{surface tension force}} = \frac{\rho_l u_b^2 d}{\sigma} \quad (3)$$

$$\mathrm{M_o} = \mathrm{E_o}\frac{\mathrm{W_e^2}}{\mathrm{Re^4}} = \frac{g\mu_l^4}{\rho_l \sigma^3} \quad (4)$$

$$\mathrm{C_D} = \frac{\mathrm{W_e}}{\mathrm{E_o}} = \frac{4gd}{3u_b^2} \quad (5)$$

$$\mathrm{C_a} = \frac{\mu_l U_T}{\sigma} \quad (6)$$

$$\mathrm{F_N} = \mathrm{E_o}\left(\frac{\mathrm{R_e}}{\mathrm{C_a}}\right)^{2/3} \quad (7)$$

where ρ_l and μ_l are density and dynamic viscosity of the liquid, respectively, σ is surface tension, u_b is bubble velocity, d is tube diameter, and g is gravitational constant.

2.2.1. Continuity equation

The unsteady state continuity equation of fluid is based upon the principle of mass conservation. The general formula of the unsteady-state continuity equation is [24, 25]:

$$\frac{\partial \rho}{\partial t} + \nabla.(\rho \vec{v}) = 0 \quad (8)$$

2.2.2. Gas volumetric fraction equation

The unsteady state gas volumetric fraction equation in 2D can be presented by the following equation [24]:

$$\frac{\partial \alpha_g}{\partial t} + \frac{\partial (u_{g,x}\alpha_g)}{\partial x} + \frac{\partial (u_{g,y}\alpha_g)}{\partial y} = 0 \quad (9)$$

The equation of liquid water volume fraction in the similar formula of gas (air) volume fraction, and the sum of two is equal to unity;

$$\alpha_l + \alpha_g = 1 \quad (10)$$

where $\alpha_l$and $\alpha_g$are the volumetric fraction of liquid and gas phase, respectively, t is the time, x and y, and the horizontal and vertical axes. The interface between the phases is tracked using the solution of the preceding equation for the volume fraction of one of two phases.

2.2.3. Momentum equation

In Newton's second law, it was stated that the sum of the forces acting on an element of fluid is equal to its acceleration rate of momentum change. This relates to the momentum equation, the general form of the momentum equation [24-27]:

$$p\left[\frac{\partial \vec{u}}{\partial t} + (\vec{u}.\nabla)\vec{u}\right] = -\nabla p + \nabla.(2\mu D) + \rho\vec{g} + \vec{F} \quad (11)$$

where u, p, g, and μ, are the velocity, pressure, acceleration of gravity, and dynamic viscosity, respectively. D represents the stress tensor which can be presented as:

$$D_{ij} = \frac{1}{2}\left[\frac{\partial u_j}{\partial x_i} + \frac{\partial u_i}{\partial x_j}\right] \quad (12)$$

3. Operating Conditions

The region's base and side walls are considered to be non-slip boundary conditions, whereas the top wall is supposed to be a boundary condition of the pressure outlet. The working pressure is set to be the same as the surrounding air pressure. The ambient pressure, i.e., 101.325 kPa, is set as the operating pressure, and the acceleration of gravity is assigned along the y-direction. ANSYS Fluent commercial package was utilized to solve the fluid volume's continuity, momentum, and fractions [28, 29]. The flow equations were of the second-order upwind scheme. A splitting operations algorithm solved the pressure velocity coupling [30]. The solution stability will attain a convergence without a significant loss [31]. The body force weight sketch and the implicit force curing were used to solve the pressure and improve the solution convergence. The study considers a grid independence analysis to determine the grid size necessary for replicating an initially static spherical bubble of the initial dimension. Furthermore, in order to mimic phase change material, a user-provided function was utilized to complete the fluent code. A time step of 10-4 was assigned to simulate the transient flow based on the explicit scheme.

4. Results and Discussion

4.1. Natural water

The rising velocity of a single air bubble increases with increasing the size of the bubble due to the impact of the increased buoyancy force, as presented in Fig. 2. When the bubble is wobbling (proceeding with staggering motion), the rising velocity at the beginning decreases and, after that, increases smoothly. During the air bubble oscillation, the rising bubble velocity was decreased at the zone of the oscillating spherical cap. In the end, the rising bubble velocity was increased at the zone of the spherical cap due to the reduction in the shape oscillation and reached to a constant value, as shown in Fig. 3.

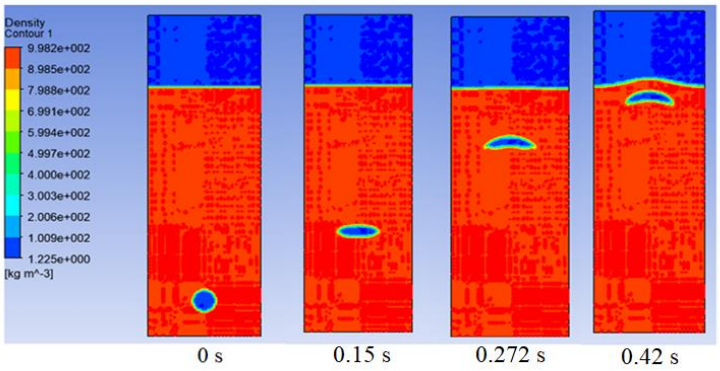

Fig. 2. Density contour for large bubble size with different time.

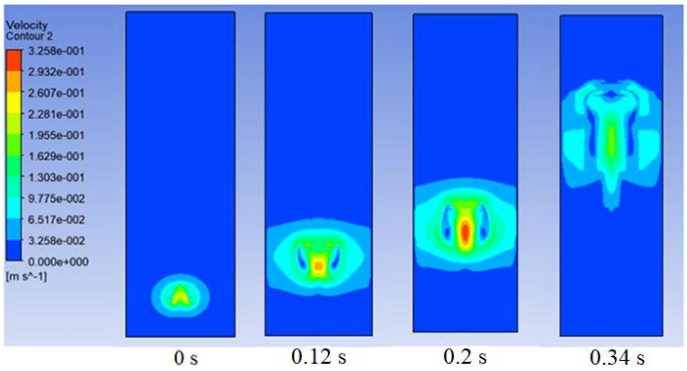

Fig. 3. Rising velocity contour with different times of simulation.

The CFD results of a single air bubble rising through a natural water column with different bubble sizes of (dB=5, 6, and 7 mm) through column dimensions (H=90 mm, W=30 mm) are depicted in Fig. 4.

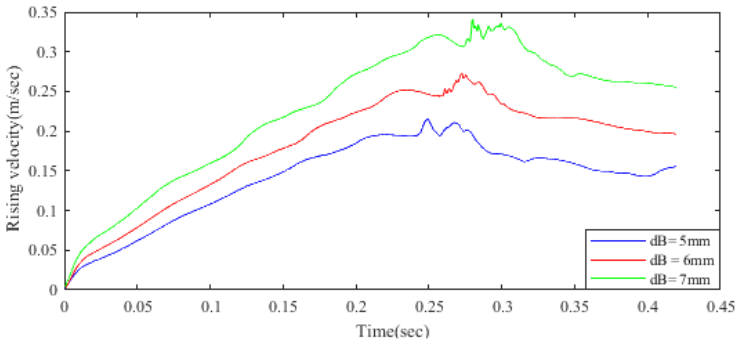

Fig. 4. Time evolution of rising velocity with different bubble size.

Figure 5 shows the rising velocity of a single air bubble rising freely in sluggish water as a function of the period from 0 to 0.42 s. The rising velocity becomes higher with increasing Eötvös number in the range 700, 800, and 950.

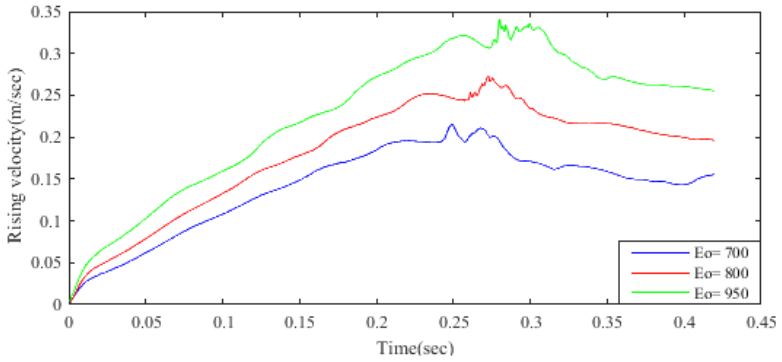

Fig. 5. Time evolution of rising velocity with different Eötvös number.

Figure 6 shows the relation between Reynolds numbers of rising of single air bubble freely in sluggish water as a time-dependent variable period from 0 to 0.42 s for different bubble sizes. The increase in bubble size increases the Reynolds number.

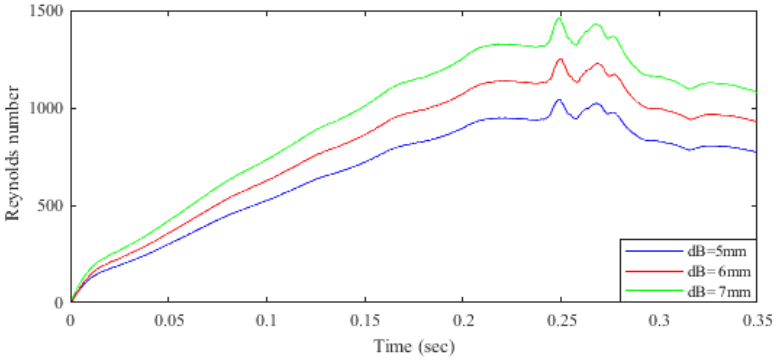

Fig. 6. Reynolds number as a function of time with different bubble size.

Figure 7 shows the Reynolds number of rising of a single air bubble freely in sluggish water as a time-dependent variable period from 0 to 0.42 s with different Eötvös numbers (700, 800, and 950). The Reynolds number increases with the increase in Eötvös number.

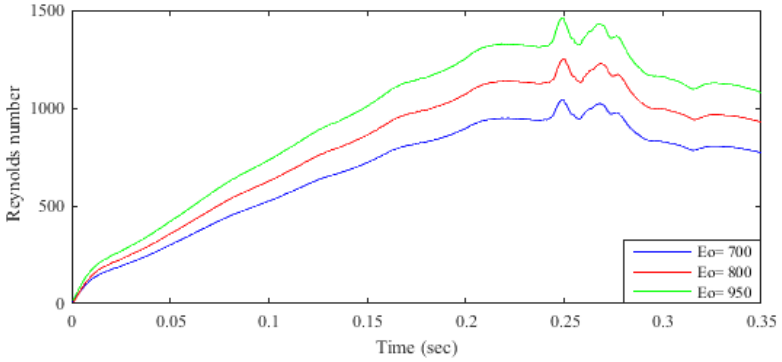

Fig. 7. Reynolds number as a function of time with different Eötvös number.

Figure 8 shows Weber number of rising of single air bubble freely in sluggish water as a time-dependent variable period from 0 to 0.42 s with different bubble sizes ranging (5, 6, and 7 mm). The Weber number increases with increased bubble size.

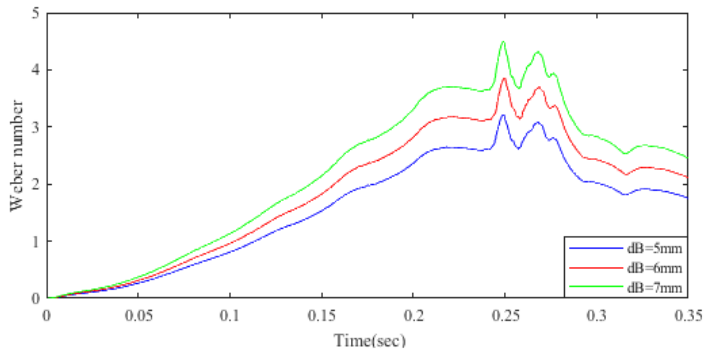

Fig. 8. Weber number as a function of time with different bubble size.

Figure 9 shows the Weber number for rising of a single air bubble freely in sluggish water as a function of the Reynolds number with different bubble sizes (5, 6, and 7 mm). The Weber number decreases with increased bubble size.

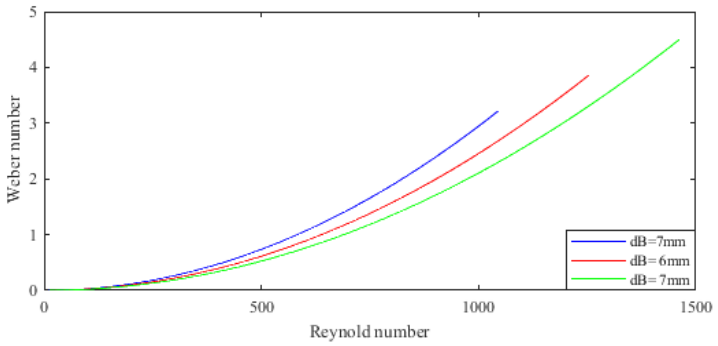

Fig. 9. Variation of Weber number with Reynolds number for different bubble size.

Figure 10 shows the Flow number for rising single air bubble freely in sluggish water as a function of the Reynolds number with different bubble sizes (5, 6, and 7 mm). The Flow number increases with increasing the size of the air bubble.

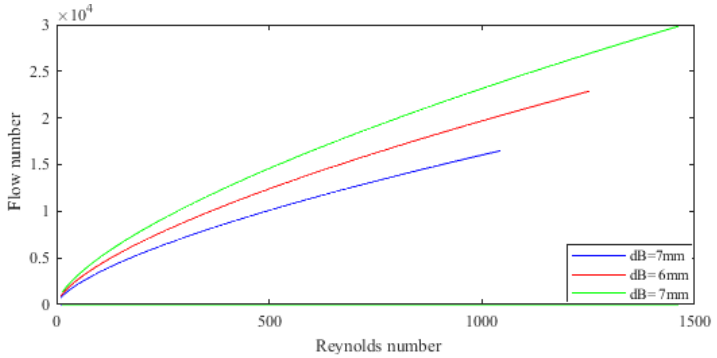

Fig. 10. Variation of Flow number with Reynolds number for different bubble size.

Figure 11 shows the drag coefficient of a single air bubble rising freely in stagnant water as a function of Reynolds number of 20 to 1475. The drag coefficient becomes smaller as the Reynolds number becomes higher in the region of Reynolds number of 20 to 1475, and it is in the range from 0.4 to 2.85.

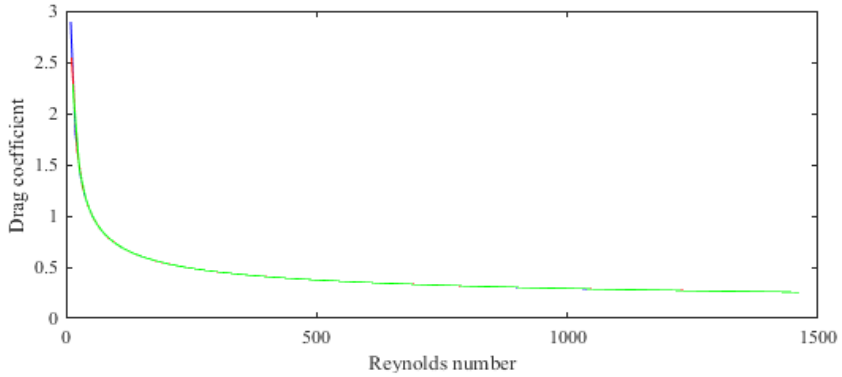

Fig. 11. Drag coefficient as a function of Reynolds number.

The CFD results of a single air bubble rising through the natural water column with a constant bubble size of (dB=5 mm) and different aspect ratios (AR=2, 3, and 4) through column dimensions of constant height (H=90 mm) and different widths (45, 30, and 22.5), respectively are depicted in Fig. 12. From this figure, the increase in aspect ratio increases the rising velocity of the air bubble. Figure 12 reveals bubble rising velocity variation with time at different bubble aspect ratios. It is clear that the higher aspect ratio gives a higher rising velocity at the initial time due to the low flow drag. The air bubble's rising velocity is affected by the initial bubble shape. The development of the final bubble shape is affected by the initial bubble shape in the flow regime. When the aspect ratio of the initial bubble shape is lower, the cap bubble is transformed into a spherical cap bubble. When the aspect ratio of the initial bubble shape is higher, the toroidal bubble is developed. The findings of this study might help researchers better grasp the design and real physical phenomena of an air bubble rising through a water column.

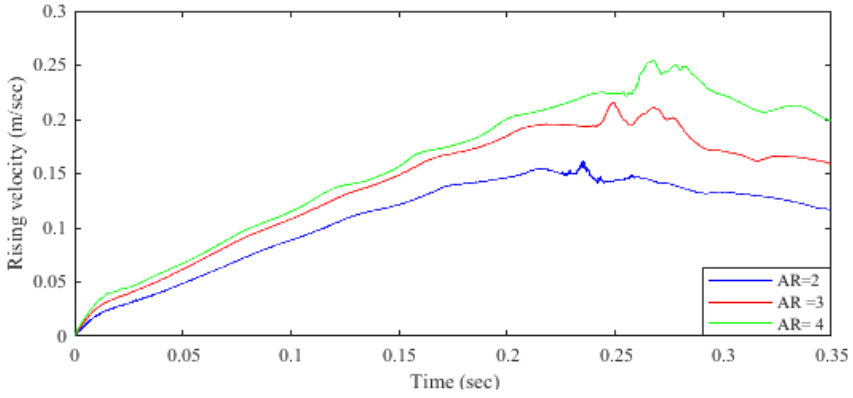

Fig. 12. Rising velocity as a time-dependent variable for different aspect ratio.

Figure 13 shows the Reynolds number of rising of a single air bubble freely in sluggish water as a time-dependent variable with different Aspect ratios (2, 3, and 4). The increase in the Aspect ratio increases the Reynolds number.

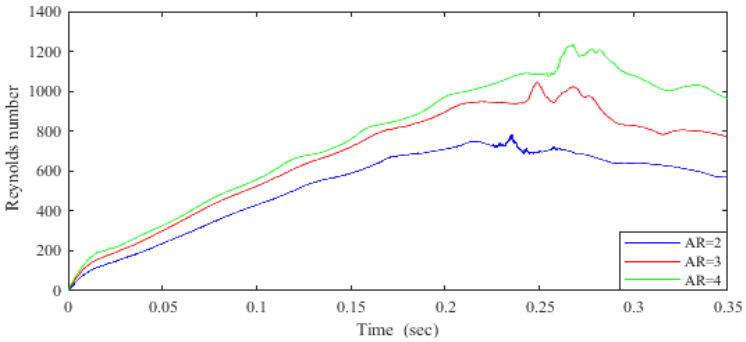

Fig. 13. Variation of Reynolds number with time for different aspect ratio.

4.2. Water with different salinity

The CFD results of a single air bubble rising through different salinity water columns (10%, 20%, and 30%) with a constant bubble size of (dB=5) through column dimensions (H=90 mm, W=30 mm) are depicted in Fig. 8. The salinity water's physical properties are reported in Table 2.

Table 2. Physical properties of water with different salinity.

Salinity (%)	Density (kg/m^3)	Kinematic viscosity (m^2/s)	Dynamic Viscosity (Pa.s)	Surface tension (N/m)
10	998.626	0.961×10^{-6}	0.000959	0.072949
20	998.707	0.987×10^{-6}	0.000985	0.072951
30	998.787	1.013×10^{-6}	0.001011	0.072953

Figure 14 shows the Reynolds number for rising single air bubble freely in the sluggish water of different salinity as a function of time. From this figure, the increase in the salinity of water decreases the Reynolds number.

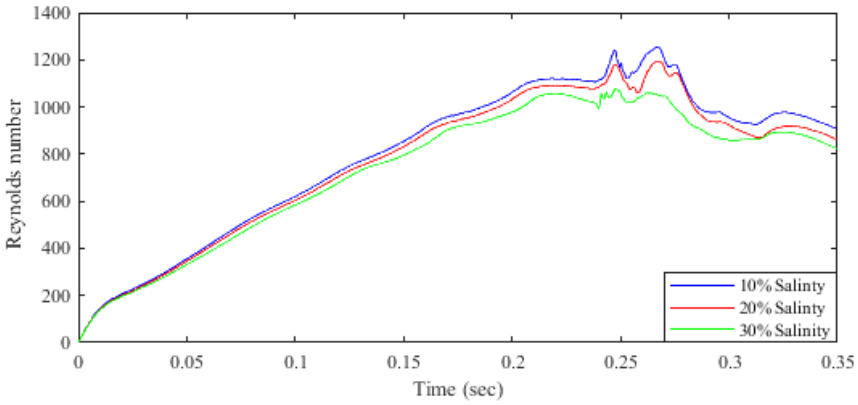

Fig. 14. Reynolds number as a function of time with different salinity.

Figure 15 shows the Weber number for rising single air bubbles freely in the sluggish water of different salinity as a function of the Reynolds number. From this figure, the increase in the salinity of the water increases Weber number.

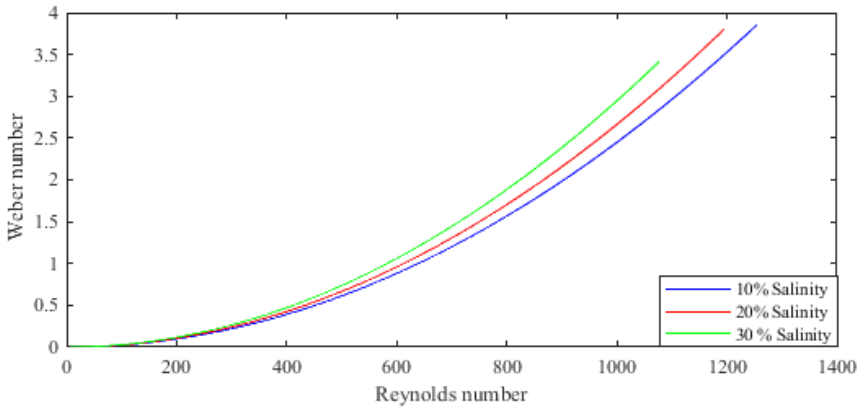

Fig. 15. Weber number vs. Reynolds number for different salinity.

Figure 16 shows the Flow number for rising single air bubbles freely in the sluggish water of different salinity as a function of the Reynolds number. From this figure, the increase in the salinity of the water increases the Flow number.

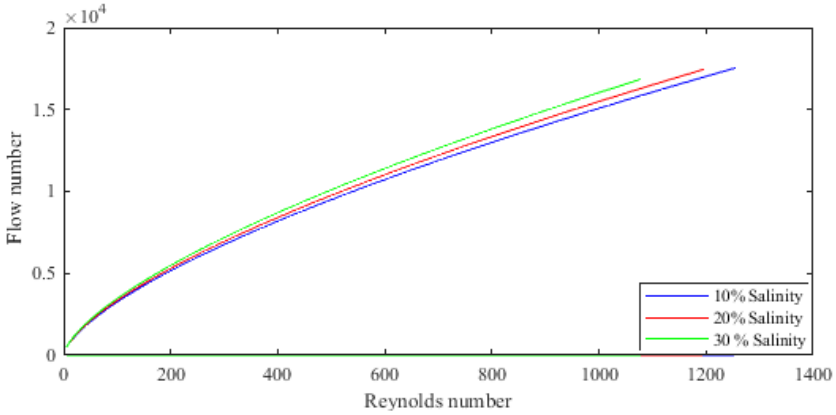

Fig. 16. Flow number vs. Reynolds number for different salinity.

5. Conclusions

The liquid (water) is used to cool most industrial operations, including refineries, petrochemical plants, LNG plants, and power plants. In this work, three different diameters (sizes) of air bubbles (5, 6, and 7 mm) rising in the water column with different salinity (10, 20, and 30 %) were numerically studied by using the Volume of Fluid (VOF) method together with the CFD technique was employed for simulating. The dynamic meshing technique is applied to simulate the hydrodynamics of rising air bubbles in liquid water columns with different salinity. It is clear that the higher aspect ratio gives a higher rising velocity at the initial time due to the low flow drag. The development of the final bubble shape is affected by

the initial bubble shape in the flow regime—also, the Reynolds number increase when the bubble size increases, while the Weber number decreases. Finally, the effect of salinity of the water decreases the Reynolds number while the Weber number increases. Moreover, the increment in the salinity of water enhances the Flow number. This study showed that there is still a need for further comparisons of FLUENT code calculations with experimental data and a sensitivity analysis of the main parameters.

Acknowledgment

This publication was funded by the Deanship of Scientific Research of Prince Sattam bin Abdulaziz University in Alkharj, Saudi Arabia.

Nomenclatures

AR	Aspect Ratio
C_a	Capillary number
C_D	Drag coefficient
D	Stress tensor, 1/s
d	Tube diameter, m
$\mathrm{E_o}$	Eötvös number
F_N	Flow number
g	Gravitational constant, m/s^2
H	Water column height, m
$\mathrm{M_o}$	Morton number
p	Pressure, N/m^2
Re	Reynolds number
T	Time, s
u_b	Bubble velocity, m/s
x and y	Horizontal and vertical axes
W	Water column width, m
$\mathrm{W_e}$	Weber number

Greek Symbols

α_l	The liquid water volume fraction
σ	Surface tension, N/m
ρ_l	Density of liquid, Kg/m^3
μ_l	Dynamic viscosity of the liquid, Pa.s

Subscript

b	Bubble
g	Gas
l	Liquid

Abbreviations

CCS	Carbon Capture and Storage
CFD	Computational Fluid Dynamics
SHMP	Sodium Hexametaphosphate
SS	Sodium Silicate

UDF	User-Defined Function
VOF	Volume of Fluid

References

1. Kugou, N.;Ishid, K.; and Yoshida, A. (2003). Experimental study on motion of air bubbles inseawater (terminal velocity and drag coefficient of air bubble rising in seawater).*Transactions on the Built Environment*, 68, 145-158.
2. Ngoh, J.; and Lim, E.W.C. (2016). Effects of particle size and bubbling behavior on heat transfer in gas fluidized beds. *Applied Thermal Engineering*, 105, 225-242.
3. Cano-Pleite, E.; Hernández-Jiménez, F.; De Vega, M.; and Acosta-Iborra, A. (2014). Experimental study on the motion of isolated bubbles in a vertically vibrated fluidized bed. *Chemical Engineering Journal*, 255, 114-125.
4. Gnyloskurenko, S.; Byakova, A.; Nakamura, T.; and Raychenko, O. (2005). Influence of wettability on bubble formation in liquid. *Journal of Materials Science*, 40(9-10), 2437-2441.
5. Sagert, N.H.; and Quinn, M.J. (1977). Influence of high-pressure gases on the stability of thin aqueous films. *Journal of Colloid and Interface Science*, 61(2), 279-286.
6. Lau, R.; Mo, R.; and Sim, W.S.B. (2010). Bubble characteristics in shallow bubble column reactors. *Chemical Engineering Research and Design*, 88(2), 197-203.
7. Ribeiro Jr., C.P.; and Lage, P.L.C. (2004). Experimental study on bubble size distributions in a direct-contact evaporator. *Brazilian Journal of Chemical Engineering*, 21(1), 69-81.
8. Talvy, C.A.; Shemer, L.; and Barnea, D. (2000). On the interaction between two consecutive elongated bubbles in a vertical pipe. *International Journal of Multiphase Flow*, 26(12), 1905-1923.
9. Liao, Y.; Rzehak, R.; Lucas, D.; and Krepper, E. (2015). Baseline closure model for dispersed bubbly flow: Bubble coalescence and breakup. *Chemical Engineering Science*, 122, 336-349.
10. Brabcová, Z.; Karapantsios, T.; Kostoglou, M.; Basařová, P.; and Matis, K. (2015). Bubble-particle collision interaction in flotation systems. *Colloids and Surfaces A: Physicochemical and Engineering Aspects*, 473, 95-103.
11. Vélez-Cordero, J.R.; Sámano, D.; Yue, P.; Feng, J.J.; and Zenit, R. (2011). Hydrodynamic interaction between a pair of bubbles ascending in shear-thinning inelastic fluids. *Journal of Non-Newtonian Fluid Mechanics*, 166(1-2), 118-132.
12. Hallez, Y.; and Legendre, D. (2011). Interaction between two spherical bubbles rising in a viscous liquid. *Journal of Fluid Mechanics*, 673, 406-431.
13. Costigan, G.; and Whalley, P.B. (1997). Measurements of the speed of sound in air-water flows. *Chemical Engineering Journal*, 66(2), 131-135.
14. Thoroddsen, S.T.; Etoh, T.G.; and Takehara, K. (2008). High-speed imaging of drops and bubbles. *Annual Review of Fluid Mechanics*, 40, 257-285.

15. Islam, M.T.; Ganesan, P.; Sahu, J.N.; Uddin, M.N.; and Mannan, A.(2015). A single air bubble rise in water: A case study. *Mechanical Engineering Research Journal*, 9, 1-6.
16. Pradeep, A.; Sharma, A.K.; Rajiniganth, M.P.; Malathi, N.; Sivaramakrishna, M.; Ponraju, D.; Nashine, B.K; .and Selvaraj, P. (2019). Numerical and experimental investigation of air-water system to simulate bubble dynamics in liquid sodium pool. *Brazilian Journal of Chemical Engineering*, 36(4), 1475-1485.
17. Nguyen, T.H.T.; Park, S.W.; and Ahn, J.-K.(2020). Properties of rising multiple CO_2 droplets under contamination of SO_2: Understanding scenarios of leakage to seawater. *Environmental Science, Journal of Coastal Research*, 36(4), 805-811.
18. Li, Y.; Ren, S..; Zhang, S.; Jiang, X.; and Pan, C. (2022). Bubble characteristics in subcooled flow boiling of seawater. *Chemical Engineering Journal*, 430, 132019.
19. Suyantara, G.P.W.; Hirajima, T.; Miki, H.; and Sasaki, K.(2020). Bubble interactions with chalcopyrite and molybdenite surfaces in seawater. *Minerals Engineering*, 157(1), 106536.
20. Ramirez, A.; Gutierrez, L.; and Laskowski, J.S. (2020). Use of "oily bubbles" and dispersants in the flotation of molybdenite in fresh and seawater. *Minerals Engineering*, 148, 106197.
21. Pham, L.H.H.P.; Rusli, R.; Shariff, A.M.; and Khan, F.(2020). Dispersion of carbon dioxide bubble release from shallow subsea carbon dioxide storage to seawater. *Continental Shelf Research*, 196, 104075.
22. Straatman, P.J.T.; and van Sark, W.G.J.H.M. (2021). Indirect air CO_2 capture and refinement based on OTEC seawater outgassing. *iScience*, 24(7), 102754.
23. Fan, L.-S.; and Tsuchiya, K. (1990). *Bubble wake dynamics in liquids and liquid-solid suspensions*. Butterworth-Heinemann.
24. Webber, N.B. (1971). *Fluid mechanics for civil engineers*. Chapman and Hall, London.
25. Rashid, F.L.; Talib, S.M.; Hussein, A.K.; and Younis, O. (2022). An experimental investigation of double pipe heat exchanger performance and exergy analysis using air bubble injection technique. *Jordan Journal of Mechanical and Industrial Engineering*, 16(2), 195-204.
26. Hussein, E.Q.; Rashid, F.L.; Hussein, A.K.; and Younis, O. (2021). Hydrodynamics of single bubble rising through water column using volume of fluid (VOF) method. *Journal of Thermal Engineering*, 7(14), 2107-2114.
27. Talib, S.M.; Rashid, F.L.; and Eleiwi, M.A.(2021). The effect of air injection in a shell and tube heat exchanger. *Journal of Mechanical Engineering Research and Developments*, 44(5), 305-317.
28. A. Fluent (2010). User's Guide. ANSYS 14.0.
29. ANSYS Inc. Fluent, 2010: http://www.Ansys.Com/Products/Fluid-Dynamics/ Fluent/
30. Akhtar, A.; Pareek, V.; and Tadé, M. (2007). CFD simulations for continuous flow of bubbles through gas-liquid columns: application of VOF method. *Chemical Product and Process Modeling*, 2(1), 1-19.
31. Issa, R.I. (1986). Solution of the implicitly discretized fluid flow equations by operator-splitting. *Journal of Computational Physics*, 62, 40-65.